

Disentangling neocortical alpha/beta and hippocampal theta/gamma oscillations in human episodic memory formation

Benjamin J. Griffiths^{1,2,3}, María Carmen Martín-Buro^{4,5}, Bernhard P. Staresina^{1,2}, & Simon Hanslmayr^{1,2,6}

1) School of Psychology, University of Birmingham, UK

2) Centre for Human Brain Health, University of Birmingham, UK

3) Department of Psychology, Ludwig-Maximilians-University, Munich, Germany

4) Laboratory of Cognitive and Computational Neuroscience (UCM-UPM), Center for Biomedical Technology, 28223 Pozuelo de Alarcón, Madrid, Spain

5) Faculty of Health Sciences, King Juan Carlos University, 28922 Alcorcón, Madrid, Spain

6) Institute for Neuroscience and Psychology, University of Glasgow, UK

Contact Information / Corresponding Authors

Benjamin J. Griffiths: benjamin.griffiths.psy@gmail.com

Simon Hanslmayr: simon.hanslmayr@glasgow.ac.uk

Abstract: 218 words

Main text: 5,458 words

Number of figures: 4

Number of pages: 15

38 Abstract

39 To form an episodic memory, we must first process a vast amount of sensory information about a to-
40 be-encoded event and then bind these sensory representations together to form a coherent memory. While
41 these two cognitive capabilities are thought to have two distinct neural origins, with neocortical alpha/beta
42 oscillations supporting information representation and hippocampal theta-gamma phase-amplitude
43 coupling supporting mnemonic binding, evidence for a dissociation between these two neural markers is
44 conspicuously absent. To address this, seventeen human participants completed a sequence-learning task
45 that first involved processing information about three stimuli, and then binding these stimuli together into
46 a coherent memory trace, all the while undergoing MEG recordings. We found that decreases in neocortical
47 alpha/beta power during sequence perception, but not mnemonic binding, correlated with enhanced
48 memory performance. Hippocampal theta/gamma phase-amplitude coupling, however, showed the
49 opposite pattern; increases during mnemonic binding (but not sequence perception) correlated with
50 enhanced memory performance. These results demonstrate that memory-related decreases in neocortical
51 alpha/beta power and memory-related increases in hippocampal theta/gamma phase-amplitude coupling
52 arise at distinct stages of the memory formation process. We speculate that this temporal dissociation
53 reflects a functional dissociation in which neocortical alpha/beta oscillations could support the processing
54 of incoming information relevant to the memory, while hippocampal theta-gamma phase-amplitude
55 coupling could support the binding of this information into a coherent memory trace.

56 Introduction

57 An episodic memory is a personal detail-rich, long-term memory that is anchored to a unique point in
58 time and space (Tulving, 2002). The formation of these memories are thought to rely on both neocortical
59 alpha/beta and hippocampal theta/gamma oscillations (Hanslmayr et al., 2016), both of which are prevalent
60 in a wide range of human episodic memory tasks (for reviews, see Hanslmayr & Staudigl, 2014; Nyhus &
61 Curran, 2010).

62 Neocortical alpha/beta desynchrony is thought to be beneficial for information representation
63 (Hanslmayr et al., 2012). This idea is derived from the tenets of information theory, which propose that
64 unpredictable states (e.g., a desynchronised network, where the firing of one neuron cannot predict the
65 firing of another) convey substantially more information than predictable states. In direct support of this
66 idea, neocortical alpha/beta (8-20Hz) power decreases have been shown to correlate with the enhanced
67 fidelity of neural representations present in BOLD signal (Griffiths, Mayhew, et al., 2019). Moreover,
68 interfering with these power decreases via transcranial magnetic brain stimulation impairs episodic memory
69 formation (Hanslmayr et al., 2014). Together, these findings (see also Fellner et al., 2013; Griffiths et al.,
70 2021; Karlsson et al., 2020; Long & Kahana, 2015; Martín-Buro et al., 2020; Sederberg et al., 2007) suggest
71 that alpha/beta power decreases are intimately tied to the successful representation of information
72 pertaining to episodic memories.

73 Hippocampal theta and gamma oscillations also play a pivotal role in episodic memory formation (e.g.
74 Bahramisharif, Jensen, Jacobs, & Lisman, 2018; Heusser, Poeppel, Ezzyat, & Davachi, 2016; Staudigl &
75 Hanslmayr, 2013; Tort, Komorowski, Manns, Kopell, & Eichenbaum, 2009). The phase of theta is thought to
76 determine whether long-term potentiation (LTP) or long-term depression (LTD) occurs (Hasselmo et al.,
77 2002), and gamma synchronisation compliments this process by driving neurons to fire at the frequency
78 optimal for spike-timing dependent plasticity (STDP; Bi & Poo, 1998; Jutras, Fries, & Buffalo, 2009; Nyhus &
79 Curran, 2010). By combining these two phenomena, hippocampal theta-gamma phase-amplitude coupling

80 is well-suited for mnemonically binding disparate sources of information into a coherent memory trace
81 (Hanslmayr et al., 2016; Lisman & Jensen, 2013).

82 On a cognitive level however, many paradigms probing human episodic memory formation involve
83 substantial overlap in information representation and mnemonic binding, making it difficult to conclude
84 that their associated neural phenomena are truly dissociable. Here, we addressed this problem by using a
85 paradigm that invokes a temporal shift in the ratio of these cognitive processes. Seventeen participants
86 were briefly presented with a sequence of three stimuli (always consisting of an object, a feature and a
87 scene), and then given a small window to intentionally bind these stimuli together for a later associative
88 memory test*. We hypothesised that memory-related changes in neocortical alpha/beta activity would
89 show a distinct temporal dynamic to memory-related changes in hippocampal theta/gamma activity.
90 Specifically, that (1) memory-related neocortical alpha/beta power decreases would be most prevalent
91 during the perception of the sequence (from here on termed “sequence perception”), as this requires
92 extensive processing of the details of each item prior to binding, and (2) memory-related increases in
93 hippocampal theta-gamma phase-amplitude coupling would be most prevalent when participants
94 intentionally associate the stimuli together (from here on termed “mnemonic binding”), given that theta-
95 gamma coupling is a proxy for forms of long-term potentiation. Indeed, the results reported below support
96 these hypotheses, suggesting that neocortical alpha/beta desynchrony and hippocampal theta/gamma
97 synchrony arise at distinct stages of the memory formation process.

98 **Materials and Methods**

99 *Participants*

100 Twenty-eight participants were recruited (mean age = 25.4; age range = 20-33; 68% female; 82% right-handed).
101 These participants received course credit or financial reimbursement in return for their participation. One participant
102 was excluded for excessive head movement (greater than 2 standard deviations above group mean). Four participants
103 were excluded for poor data quality (more than 50% of trials rejected for artifacts). Six participants were excluded for
104 extreme memory performance (fewer than 15 trials in one of the three memory conditions). This left seventeen
105 participants for further analysis (mean age = 24.9; age range = 20-32; 65% female; 82% right-handed). Ethical approval
106 was granted by the Research Ethics Committee at the University of Birmingham (ERN_15-0335), complying with the
107 Declaration of Helsinki.

108 *Experimental design*

109 Each participant completed a visual associative memory task (see figure 1a). During encoding, participants were
110 presented with a line drawing of an object, a pattern, and a scene (each for 1500ms, with a jittered 600ms (± 100 ms)
111 fixation cross shown between each stimulus). Participants were then given a short interval to create a mental image
112 incorporating the three stimuli to help them recall the stimuli for a later memory test. Participants were then asked to
113 rate how difficult they found associating the triad. This question was used to keep participants attending to the task,
114 rather than provide a meaningful metric for analysis. The next trial began after the participant had responded to the
115 difficulty question. After associating 48 triads, participants started the distractor task. In the distractor task,
116 participants attended to a fixation cross in the centre of a black screen. The fixation cross would flash momentarily
117 (~ 100 ms) from light grey to either white or dark grey approximately every 20 seconds. The participants were instructed
118 to count the number of times the fixation cross changed to white (ignoring the times it turned dark grey) and report
119 this value at the end of the task (approximately 2.5mins later). The retrieval task followed the distractor. Here,

* While it is impossible to conclude with absolute certainty that perception and mnemonic binding are completely separable in any memory task, here we can conclude that there is a substantial shift in the ratio of the two processes. Stimulus perception will only be taking place while there is stimulus to perceive (i.e., during the presentation of the sequence), while mnemonic binding will be most prevalent when all sequence items have been presented and processed (i.e., after the final stimulus has been processed by the cortex). While this leaves room for some binding to occur towards the very end of the presentation of the last stimulus, this would be minimal in comparison to what follows during the “binding window” (see figure 1a, outlined in red). Direct contrasts of the MEG signals between sequence perception and mnemonic binding will empirically test this hypothesised shift in ratio.

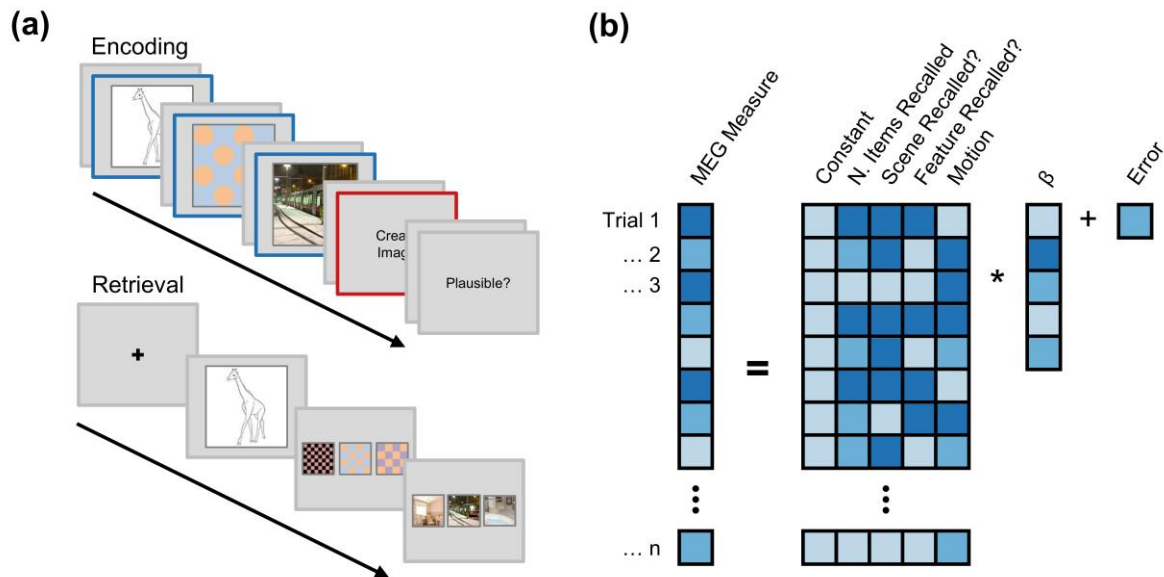


Figure 1. Overview of task and analytical approach (a) Paradigm schematic. Participants were presented with a sequence of three visual stimuli. The sequence always began with a line drawing of an object, and was then followed by a pattern and a scene (each with a brief fixation cross shown between). Participants were then given a short interval to create a mental image incorporating the three stimuli, before being asked to rate how difficult it was to create the association. After a distractor task, participants were presented with the object as a cue and asked to recall both the pattern and the scene, each from a choice of three stimuli. After selection, participants had to rate how confident they felt about their response. The epochs representing “sequence perception” are outlined in blue, and the epoch representing “mnemonic binding” is outlined in red. (b) Analysis schematic. For each participant, spectral power and theta-gamma phase-amplitude coupling were modelled using a general linear model including predictors for the number of items recalled, scene and feature memory recall, and head motion. The resulting standardised beta coefficient for the central predictor (i.e., number of items recalled) was extracted, pooled across participants, and subjected to a one sample t-test to determine whether the number of items recalled predicted changes in spectral power and/or theta-gamma coupling.

120 participants were presented with the line drawing (for 3000ms) and asked to recall the mental image they made during
 121 the encoding phase. Then, participants were presented with three patterns (one correct and two lures) and asked to
 122 identify the pattern associated with the line drawing. After responding, participants were presented with three scenes
 123 (one correct and two lures) and again asked to identify the pattern associated with the line drawing. After responding,
 124 participants were then asked to indicate how confident they were about their choices. They could select ‘guess’ (i.e.,
 125 they guessed their choice), ‘unsure’ (i.e. they could not remember the item, but had a feeling it was the correct choice),
 126 or ‘certain’ (i.e. they could vividly remember the item). Participants were asked to recall all 48 triads learnt in the earlier
 127 encoding phase.

128 Participants completed four blocks of this task (192 trials in total). The order in which the pattern and scene were
 129 presented during perception was swapped between each block (where a “block” is defined as a complete cycle of
 130 encoding, distractor and retrieval tasks). On blocks where scenes preceded patterns during perception, the
 131 presentation order at retrieval was also reversed.

132 For all responses, participants used two non-magnetic, single-finger optical response pads. The left pad allowed
 133 participants to cycle through the possible responses, and the right pad allowed participants to confirm their selection.

134 *Behavioural analysis*

135 For each trial, memory performance was coded as either ‘complete’ (i.e., they remembered both the scene and
 136 the pattern), ‘partial’ (i.e. they remembered only one of the associates), or ‘forgotten’ (i.e. they remembered neither
 137 the scene nor the pattern). Any selection where the participant indicated that they guessed was marked as a ‘miss’.

138 *MEG acquisition*

139 MEG data was recorded using a 306-channel (204 gradiometers, 102 magnetometers) whole brain Elekta
 140 Neuromag TRIUX system (Elekta, Stockholm, Sweden) in a magnetically shielded room. Participants were placed in the
 141 supine position for the duration of the experiment. Data was continuously recorded at a sampling rate of 1000Hz. The

142 head shape of each participant (including nasion and left/right ear canal) was digitised prior to commencing the
143 experiment. Continuous head position indicators (cHPI) were recorded throughout. The frequencies emitted by the
144 cHPI coils were 293Hz, 307Hz, 314Hz and 321Hz. Magnetometer data was excluded from the main analysis as they
145 contained substantial noise that could not be effectively removed or attenuated.

146 *MEG preprocessing*

147 All data analysis was conducted in Matlab using Fieldtrip (Oostenveld et al., 2011) in conjunction with custom
148 scripts. First, the data was lowpass filtered at 165Hz to remove the signal generated by the HPI coils. Second, the data
149 was epoched around each event of interest. At encoding, the epochs reflected the time windows where each stimulus
150 was presented (from here on termed 'sequence perception') and when the 'associate' prompt was presented (termed
151 'mnemonic binding'). Sequence perception epochs began 2000ms before stimulus onset and ended 3500ms after
152 onset (that is, 2000ms after stimulus offset). Mnemonic binding epochs began 2000ms before stimulus onset and
153 ended 5000ms after onset (that is, 1500ms after stimulus offset). Third, independent components analysis was
154 conducted, and any identifiable eye-blink or cardiac components were removed. Fourth, the data was visually
155 inspected, and any artefactual epochs or sensors were removed from the dataset (mean percentage of trials removed:
156 18.0%; range: 5.7-32.2%).

157 *Movement correction*

158 To identify participants with extreme head motion during MEG recordings, the recorded data was first highpass
159 filtered to 250Hz to isolate the cHPI signal. Second, the variance of the signal for each sensor was computed across
160 every time point of the continuous recording. Third, the variance was mean averaged across sensors to provide a
161 singular estimate of change in cHPI signal across the duration of the experiment. Fourth, the mean variance and its
162 standard deviation was calculated across participants. Lastly, participants with extreme head motion were identified
163 as those with variance greater than two standard deviations above the group mean. These participants were excluded
164 from further analysis.

165 To help attenuate motion-related confounds in the spectral power and phase-amplitude coupling analyses, a
166 trial-by-trial estimate of motion was calculated. First, the data was highpass filtered at 250Hz. Second, the data was
167 epoched into trials matching those outlined in the section above. Third, the envelope of the signal in each epoch was
168 calculated (to avoid issues of mean phase angle difference in cHPI signal across trials). Fourth, the envelope was
169 averaged over time to provide a single value for each epoch and channel. Fifth, the dot product was computed across
170 sensors between the first epoch and every other epoch (algebraically: $\sum_{i=1}^n a_i b_i$, where n is the number of channels,
171 a_i is the power at sensor i during the first trial, and b_i is the power at sensor i during the trial of interest). This provided
172 a single value (between zero and infinity) for each trial that described how similar the topography of that trial was to
173 the first trial – the higher the value, the more similar the topographies are between the two trials (with the assumption
174 that the more dissimilar a cHPI topography is to the starting topography, the more the head has deviated from its
175 starting position). These values were entered as a regressor of no interest in the central multiple regression analyses.

176 *Time-frequency decomposition and statistical analysis*

177 Sensor-level time-frequency decomposition was conducted on the sequence perception and mnemonic binding
178 epochs. For low frequencies, the preprocessed data was first convolved with a 6-cycle wavelet (-0.5 to 3 seconds [to 2
179 seconds for perceptual epochs to avoid the subsequent stimulus], in steps of 50ms; 2 to 40Hz; in steps of 1Hz). For
180 high frequencies, Slepian multitapers were first used to estimate power (-0.5 to 3 seconds [to 2 seconds for perceptual
181 epochs], in steps of 50ms; 40 to 100Hz, in steps of 4Hz). For this latter analysis, frequency smoothing was set to one
182 quarter of the frequency of interest and temporal smoothing was set to 200ms. Second, planar gradiometers were
183 combined by summing the power of the vertical and horizontal components. Third, for perceptual trials only, power
184 was then averaged over the three stimulus presentation windows of each triad to provide mean power during
185 perception of the triad. Any triads where one or more epochs had been rejected during preprocessing were excluded
186 at this stage. We averaged spectral power across the three windows as we reasoned that this approach would be most
187 sensitive to changes in spectral power that predicted the number of items later recalled. To successfully recall a
188 stimulus, an alpha/beta power decrease must arise in two of the windows – the initial line drawing (i.e. the retrieval
189 cue) and the to-be-recalled stimulus. As such, focusing analyses on a single stimulus is less sensitive to later memory

190 performance than an aggregate measure created by averaging across the epochs. Fourth, the background 1/f
191 characteristic was subtracted using an iterative linear fitting procedure.

192 To isolate oscillatory contributions, 1/f activity was attenuated in the time-frequency data by subtracting the
193 linear fit of the 1/f characteristic (Griffiths, Parish, et al., 2019; Manning et al., 2009; Zhang & Jacobs, 2015). To this
194 end, a vector containing values of each derived frequency (A) and another vector containing the power spectrum,
195 averaged over all time-points and trials of the relevant memory condition (B) were log-transformed to approximate a
196 linear function. The linear equation $Ax = B$ was solved using least-squares regression, where x is an unknown
197 constant describing the 1/f characteristic. The 1/f fit (Ax) was then subtracted from the log-transformed power
198 spectrum (B). As this fit can be biased by outlying peaks (Haller et al., 2018), an iterative algorithm was used that
199 removed probable peaks and then refitted the 1/f. Outlying peaks in this 1/f-subtracted power spectrum were
200 identified using a threshold determined by the mean value of all frequencies that sat below the linear fit. The MEG
201 power spectrum is the summation of the 1/f characteristic and oscillatory activity (i.e., at no point does oscillatory
202 activity subtract from the 1/f), therefore all values that sit below the linear fit can be seen as an estimate error of the fit.
203 Any peaks that exceed the threshold were removed from the general linear model, and the fitting was repeated.
204 Notably, as power for the low frequencies (2-40Hz) and high frequencies (40-100Hz) was calculated using different
205 methods (wavelets and Slepian multitapers, respectively), the two bands have disparate levels of temporal and spectral
206 smoothing. To avoid a spurious fitting due of the 1/f because of these differences, the 1/f correction was conducted
207 separately for these two bands.

208 For statistical analysis, a trial-based multiple regression was run for each participant. Four regressors were used
209 to predict observed power for every channel x frequency x time point independently. These four regressors were (1)
210 number of items recalled, (2) whether the scene was recalled, (3) whether the pattern was recalled, (4) the change in
211 head position [based on the motion calculation outlined above]. The first regressor was of primary interest, the second
212 and third regressors isolated spectral power changes that can be uniquely described by whether the scene/pattern
213 was recalled (respectively), and the fourth regressor accounted for changes in spectral power driven by head
214 movement (see the next paragraph for notes on multicollinearity). The beta weight of the first regressor, obtained for
215 a given channel x frequency x time point, was then standardised by dividing the standard error of the fit (providing a
216 t-value) to attenuate the impact of poor model fits on the final analysis. Here, a positive standardised beta coefficient
217 would indicate that spectral power increases with more items recalled, and a negative beta coefficient would indicate
218 that spectral power decreases with more items recalled. The beta coefficients for each participant were pooled across
219 the sample and entered into a one-tailed cluster-based permutation test (2000 permutations, alpha threshold = 0.05,
220 cluster alpha threshold = 0.05, minimum neighbourhood size = 3; Maris & Oostenveld, 2007) to examine whether the
221 observed fits consistently deviated from the null hypothesis ($t=0$) across participants. Clusters that produced a p-value
222 less than 0.05 were considered significant. Cohen's d_z was used as the measure of effect size for these clusters (Lakens,
223 2013), where $d_z = \frac{\bar{t}}{\sqrt{n}}$, \bar{t} = mean t-statistic within the cluster, n = number of participants.

224 Notably, it is plausible to suggest that the three memory regressors are, to some extent, correlated and that this
225 would introduce multicollinearity into the regression models. To test this, we calculated the Variance Inflation Factor
226 (VIF) – a measure of the magnitude of multicollinearity. Rule of thumb suggests that a VIF greater than 10 is considered
227 high and could compromise the model (Kutner et al., 2004). The VIF between number of items recalled and scene
228 recall success was, on average, 2.615 (s.d. 2.621), and the VIF between number of items recalled and pattern recall
229 success was, on average, 1.027 (s.d. 0.033). As these values fall below the threshold of 10, multicollinearity is not an
230 apparent concern.

231 An additional analysis was conducted to confirm that alpha/beta power did indeed decrease following the onset
232 of the sequence stimuli. This analysis followed the same approach as above (i.e., regression-based analyses across
233 trials for each participant individually, and then group-level statistics on the resulting standardised beta coefficients).
234 However, two changes were made: (1) the outcome variable became the change in 1/f-corrected spectral power from
235 baseline (-250ms to stimulus onset; as opposed to raw spectral power), and (2) the memory-related regressors
236 removed from the regression models, as they were of no relevance here.

237 *Source analysis*

238 The preprocessed data was reconstructed in source space using individual head models and structural (T1-
239 weighted) MRI scans for all but two individuals who did not wish to return for an MRI scan. For these two individuals,

240 a standard head model and MRI scan was used (taken from the Fieldtrip toolbox; for details, see
241 <http://www.fieldtriptoolbox.org/template/headmodel>). The head shape (together with the HPI coil positions) of each
242 participant was digitised using a Polhemus Fasttrack system. The timelocked MEG data was reconstructed using a
243 single-shell forward model and a Linearly Constrained Minimum Variance beamformer (LCMV; van Veen, van
244 Drongelen, Yuchtman, & Suzuki, 1997). The lambda regularisation parameter was set to 1%.

245 *MEG phase-amplitude coupling computation and statistical analysis*

246 For the phase-amplitude coupling analyses, we focused our analysis directly on source-reconstructed
247 hippocampal virtual sensors. Given the depth and size of the hippocampus (it makes up around ~1% of the MEG
248 sourcemodel), the likelihood that legitimate hippocampal phase-amplitude coupling can be observed on the scalp is
249 practically nil. Therefore, it makes most sense to move directly to source space and analyse source-localised measures
250 of hippocampal activity.

251 To calculate the extent to which hippocampal gamma activity coupled to hippocampal theta phase, the
252 modulation index (MI) was calculated (Tort et al., 2010). First, the peak theta and gamma frequencies were calculated
253 by estimating power across all hippocampal virtual sensors (bilaterally, as defined by the automated anatomical
254 labelling [AAL] atlas) using the same time-frequency decomposition method reported above[†]. The Matlab function
255 *findpeaks()* was then used to extract the most prominent peak within the theta (2-7Hz) and gamma (40-80Hz) bands
256 for each participant. Across participants, the mean theta peak was at 5.1Hz (standard deviation: 1.0Hz; range: 3.1-
257 7.0Hz), and the mean gamma peak was at 66.1Hz (standard deviation: 4.6Hz; range: 59.0-73.0Hz) [see supplementary
258 figure 1 for all plots]. Second, the time-series of the hippocampal virtual sensors were duplicated, with the first being
259 filtered around the theta peak (± 0.5 Hz) and the second being filtered around the gamma peak (± 5 Hz). Third, the Hilbert
260 transform was applied to the theta- and gamma-filtered time-series, with the phase of the former and power of the
261 latter being extracted. Fourth, the time-series data was re-epoched, beginning 500ms after the onset of the
262 stimulus/fixation cross and at the onset of the next screen. This attenuated the possibility that an event-related
263 potential and/or edge artifacts from the filtering/Hilbert transform could influence the phase-amplitude coupling
264 measure (Aru et al., 2014). Fifth, gamma power was binned into 12 equidistant bins of 30°, according to the concurrent
265 theta phase. This binning was conducted for each trial and sensor separately. Sixth, the MI was computed by comparing
266 the observed distribution to a uniform distribution. Seventh, the resulting MI values were subjected to a trial-based
267 multiple regression conducted in the same manner as for the spectral power analyses. However, two additional
268 regressors were added to this model: (1) hippocampal peak theta power [per trial, averaged across 500ms to 3000ms],
269 (2) hippocampal peak gamma power [per trial, averaged across 500ms to 3000ms]. These regressors addressed the
270 potential confound of concurrent power influence phase estimates (Aru et al., 2014). Eighth, these results were
271 averaged over hippocampal virtual sensors and these per-participant standardised beta coefficients were subjected to
272 a permutation-based one-sample t-test contrasting memory-related changes in phase-amplitude coupling to the null
273 hypothesis ($t=0$). Notably, as we had focused our analyses on the peak theta and gamma frequencies, and used the
274 average PAC values across virtual sensors, only a single statistical comparison was made. Therefore, no cluster-based
275 multiple comparison correction was required. As the p-values reported here are estimated by permutation rather than
276 from the parametric test, the t-values and degrees of freedom we report should only be used for reference.

277 We examined the spatial specificity of this effect by using the same pipeline as above to assess theta-gamma
278 phase-amplitude coupling in the frontal, occipital, parietal, and temporal lobes (individually; as defined by the
279 *wfupickatlas* toolbox for SPM). This analysis (plus source visualisation) help confirm that theta-gamma coupling
280 observed in the hippocampus ROI originated from the hippocampus itself, rather than “bled in” from another region.

281 To compliment this analysis, we also ran a searchlight-based analysis. Here, we aimed to contrast the magnitude
282 of the memory-related hippocampal coupling effect with memory-related coupling effects outside the hippocampus
283 (in searchlights including approximately the same number of voxels; assuaging concerns that the lobe-based ROIs were

[†] Though the notion of localising deep regions such as the hippocampus was once controversial, an ever-growing number of studies have suggested that it is achievable. Ruzich and colleagues (2019) uncovered 29 studies that used gradiometers alone to localise hippocampal signals, while Dalal and colleagues (2013) demonstrated that MEG signals directly correlate with simultaneously recorded intracranial hippocampal recordings. As such, the theoretical notion that the hippocampus cannot be measured using MEG has been refuted by numerous empirical demonstrations to the contrary.

284 too broad to detect local coupling effects). To this end, we iterated through every source voxel, identified its immediate
285 neighbours (those immediately in front of and behind the voxel in 3-dimensional space [mini-cluster size: 27 voxels;
286 for comparison, hippocampal ROI = 25 voxels]), and took the mean memory-related hippocampal phase-amplitude
287 coupling within this mini-cluster. For each mini-cluster, this mean value was then contrasted against chance, and the
288 resulting t-statistic was added to a distribution describing the magnitude of memory-related phase-amplitude coupling
289 across the brain. A p-value was then derived by comparing hippocampal coupling to the whole-brain distribution (as
290 done in a permutation test), allowing us to infer the extent to which hippocampal phase-amplitude coupling deviated
291 from what was typical within the brain.

292 Results

293 *Behavioural results*

294 Participants, on average, correctly recalled both the associated pattern and associated scene on 38.3%
295 of trials, recalled only one associated stimulus on 34.4% of trials, and failed to recall either associate on
296 27.3% of trials. Participants correctly recalled the associated pattern on 49.2% of trials, and correctly
297 recalled the associated scene on 82.1% of trials (both of which are well above chance performance [33.3%]).
298 A paired-samples t-test revealed that memory for scenes was substantially greater than memory for
299 patterns ($p < 0.001$, Cohen's $d_z = 4.31$). To attenuate the impact of differing memory performance for the
300 two stimulus types in the subsequent analyses, two regressors were included in all models that served to
301 suppress variance attributable to scene-specific and feature-specific memory.

302 *Neocortical alpha/beta power decreases during sequence perception predict enhanced memory* 303 *performance*

304 After establishing that alpha/beta power did indeed decrease from baseline following the presentation
305 of the sequence stimuli ($p_{\text{corr}} < 0.001$, Cohen's $d_z = 1.22$, cluster size = 28,260, mean t-statistic within cluster
306 = -5.03; see figure 2a/d), we set out to test our first hypothesis: are memory-related decreases in alpha/beta
307 power more prevalent during the perception of the sequence than during mnemonic binding?

308 During sequence perception, cluster-based analysis revealed a significant effect where a decrease in
309 alpha/beta power correlated with an increase in the number of items later recalled ($p_{\text{corr}} = 0.032$, Cohen's
310 $d_z = 0.60$, cluster size = 1013, mean t-statistic within cluster = -2.47; see figure 2a-f). This cluster extended
311 over the posterior sensors, bilaterally, between 8 and 15Hz (see figure 2b). Source reconstruction confirmed
312 this localisation, implicating bilateral early occipital regions (see figure 2e). Parsimonious results were found
313 during retrieval (see supplementary figure 2), and when breaking the memory effects down by stimulus
314 type (see supplementary figure 3).

315 No memory-related changes in theta power (2-7Hz; $p_{\text{corr}} = 0.101$), "slow" gamma power (40-60Hz; no
316 cluster formed), or "fast" gamma power (60-100Hz; no cluster formed) were observed during the
317 presentation of the sequence.

318 No decrease in alpha/beta power was observed when participants were asked to engage in mnemonic
319 binding ($p_{\text{corr}} = 0.413$; see figure 2g). Similarly, no memory-related changes in theta power (2-7Hz; $p_{\text{corr}} =$
320 0.130), "slow" gamma power (40-60Hz; no cluster formed), or "fast" gamma power (60-100Hz; no cluster
321 formed) were observed when participants were asked to engage in mnemonic binding.

322 A direct contrast of spectral power between sequence perception and mnemonic binding
323 demonstrated that the inverse relationship between alpha power and subsequent memory performance
324 was significantly more pronounced during perception ($p_{\text{corr}} = 0.014$, Cohen's $d_z = 0.60$, cluster size = 794,
325 cluster t-statistic = -2.49; see figure 2f). Together, these findings suggest that alpha/beta power decreases

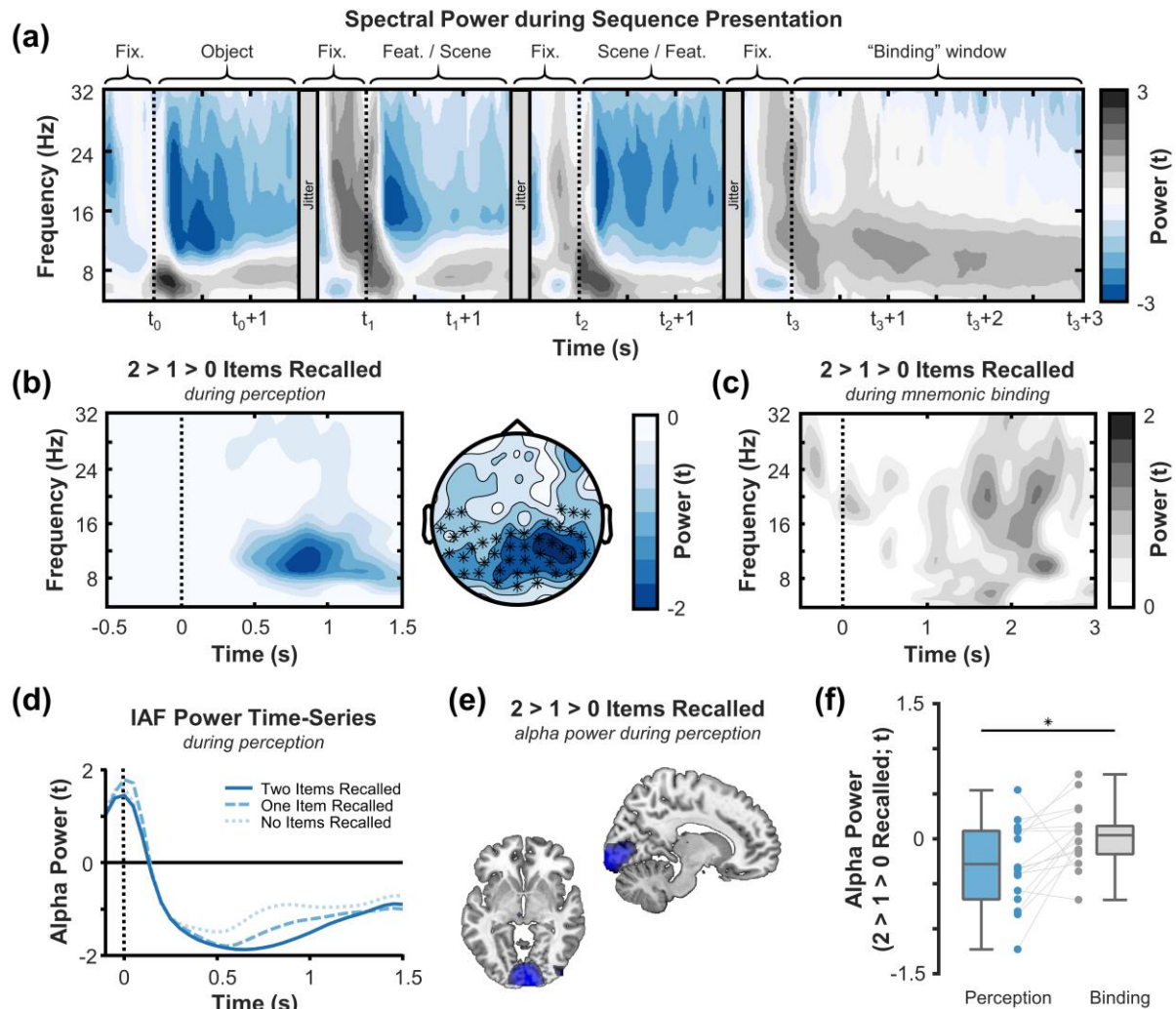


Figure 2. Neocortical alpha/beta power decreases during sequence perception scale with the number of items later recalled. (a) Time-frequency plot of alpha/beta power (averaged across all trials) during sequence presentation and subsequent binding. Alpha/beta power only decreases during sequence presentation. (b) Time-frequency plot (left) and topoplot (right) of the negative correlation between alpha/beta power during sequence perception and the number of items later recalled. The time-frequency plot uses the average of all channels included in the significant cluster (visualised by crosses in the topoplot to the right). The topoplot depicts values for time-frequency bins included in the significant cluster (i.e., 8-15Hz; 300-1300ms). (c) Time-frequency plot of the correlation between alpha/beta power during mnemonic binding and the number of items later recalled, plotted over the same channels as those visualised in panel b. No significant effect was observed. (d) Time-series plot of the power at the individual alpha frequency (IAF) of each participant for each memory condition. The more items later recalled, the greater the power decrease [$p_{corr} = 0.034$ at IAF]. (e) Source localisation of the effect in panel b. The memory-related alpha/beta power decreases during sequence perception peak in the occipital cortex. (f) Boxplot of memory-related decreases in alpha/beta power during sequence perception and mnemonic binding. Across participants, memory-related decreases in alpha/beta power were significantly greater during sequence perception than during mnemonic binding.

326 during sequence perception, but not during mnemonic binding, scale with the number of items that are
 327 later recalled.

328 *Hippocampal theta/gamma phase-amplitude coupling during mnemonic binding, but not information*
 329 *representation, predicts successful episodic memory formation*

330 We then probed how hippocampal theta/gamma phase-amplitude coupling relates to episodic
 331 memory formation. During mnemonic binding, increases in hippocampal theta/gamma phase-amplitude

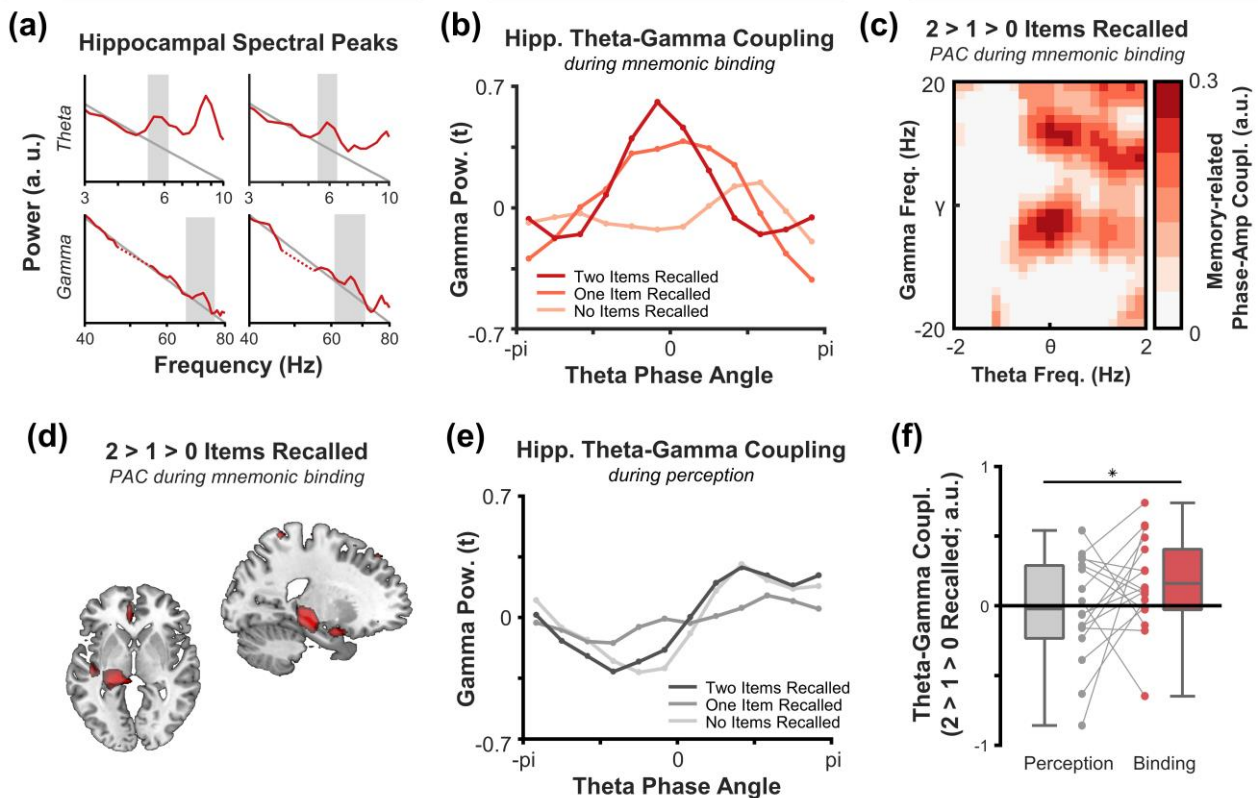


Figure 3. Increases in hippocampal theta-gamma coupling during mnemonic binding scale with the number of items later recalled. (a) Exemplar plots of peak theta and gamma frequencies for two participants (red line depicts hippocampal power; dotted red line depicts frequencies interpolated due to line noise; grey line depicts fitted 1/f component; grey area depicts identified peak). (b) Hippocampal gamma power as a function of hippocampal theta phase, for each memory condition, during the mnemonic binding window. When more items were later recalled, gamma power fluctuated in line with theta phase more noticeably. (c) Memory-related hippocampal theta-gamma coupling as a function of theta and gamma frequencies. Theta-gamma coupling appeared to peak at approximately the peak theta and gamma frequencies, supporting the idea that this coupling arises between two narrow-band oscillatory signals. (d) Theta-gamma coupling peaked in the hippocampus. To emphasise coupling patterns that were consistent across both hemispheres, the two hemispheres have been averaged together, and the averaged result visualised in the left hemisphere of the source plot. (e) Hippocampal gamma power as a function of hippocampal theta phase, for each memory condition, during sequence perception. No memory-related differences in coupling were observed. (f) Boxplot of memory-related increases in theta/gamma coupling during sequence perception and mnemonic binding. Across participants, memory-related increases in theta/gamma coupling were significantly greater during mnemonic binding than during sequence perception.

332 coupling scaled with the number of items later recalled ($t(16) = 2.24$, $p = 0.020$, Cohen's $d_z = 0.54$; see figure
 333 3). No significant coupling was observed during perception ($p > 0.5$). A direct contrast in PAC between
 334 sequence perception and mnemonic binding revealed that memory-related increases in PAC are more
 335 pronounced during mnemonic binding ($t(16) = 1.93$, $p = 0.040$, Cohen's $d_z = 0.47$). These results suggest that
 336 memory-related theta/gamma phase-amplitude coupling is most prominent during periods of mnemonic
 337 binding.

338 To ensure that the hippocampal effect observed during mnemonic binding was not a result of spatial
 339 smearing from some other region, we re-ran this analysis using four additional regions of interest: the
 340 frontal lobe, parietal lobe, temporal lobe (excluding the hippocampus), and the occipital lobe. None of these
 341 regions exhibited significant theta-gamma phase-amplitude coupling during mnemonic binding (frontal: p
 342 = 0.308, parietal: $p = 0.250$, temporal: $p = 0.078$, occipital: $p = 0.169$). Furthermore, a searchlight-based
 343 analysis revealed that hippocampal phase-amplitude coupling was substantially greater than other

344 searchlight-based regions-of-interest that matched the
345 size of the hippocampus ($p = 0.024$). Together, these
346 results suggest that the memory-related enhancement in
347 hippocampal theta/gamma phase-amplitude coupling is
348 indeed originating from the source-reconstructed
349 hippocampus, as opposed to “bleeding in” from
350 neighbouring regions.

351 As can be seen in figure 3b, there is an apparent
352 memory-related shift in the phase at which gamma
353 couples to theta during mnemonic binding. As the
354 modulation index used above is insensitive to such shifts,
355 we statistically appraised this effect using a circular-to-
356 linear correlation. Alas, no consistent change was found
357 ($p = 0.435$) suggesting that gamma activity does not
358 precess along the phase of theta as a function of the
359 number of items later recalled.

360 *A double dissociation between the timing of memory-
361 related decreases in neocortical alpha/beta power
362 decreases and memory-related increases in hippocampal
363 theta/gamma phase-amplitude coupling*

364 Lastly, we formalised the distinction between
365 memory-related neocortical alpha/beta power decreases
366 and hippocampal theta-gamma phase-amplitude
367 coupling. To this end, we conducted a 2x2 repeated
368 measures ANOVA with encoding stage (perception vs. binding) and metric (alpha/beta power decreases vs.
369 theta-gamma coupling) as factors. This revealed a significant interaction where memory-related alpha/beta
370 power decreases and memory-related theta-gamma coupling increases are dependent on the nature of the
371 ongoing cognitive task [$F(1,16) = 9.14$, $p = 0.008$, partial eta squared = 0.36] (see figure 4). There was no
372 main effect of cognitive task [$F(1,16) = 0.99$, $p = 0.33$, partial eta squared = 0.06], nor metric [$F(1,16) = 0.20$,
373 $p = 0.50$, partial eta squared = 0.03]. These results, in conjunction with those reported in the sections above,
374 suggest that a double dissociation exists between neocortical alpha/beta power decreases and hippocampal
375 theta-gamma phase-amplitude coupling, with the former being most pronounced during periods of
376 information processing and the latter being most pronounced during periods of mnemonic binding.

377 Discussion

378 Reductions in neocortical alpha/beta power and enhancements in hippocampal theta-gamma phase-
379 amplitude coupling are thought to play dissociable roles in the formation of episodic memories (Hanslmayr
380 et al., 2016), with the former supporting information representation and the latter supporting mnemonic
381 binding. As such, one would expect that these neural phenomena are temporally dissociable, with
382 alpha/beta power decreases arising first (supporting the processing of incoming information) and theta-
383 gamma phase-amplitude coupling arising later (supporting mnemonic binding, which can only arise after
384 the information has initially been processed in the cortex). Here, we found just that. Memory-related
385 decreases in neocortical alpha/beta power principally arose during sequence perception, while memory-
386 related increases in hippocampal theta/gamma phase-amplitude coupling principally arose during a time

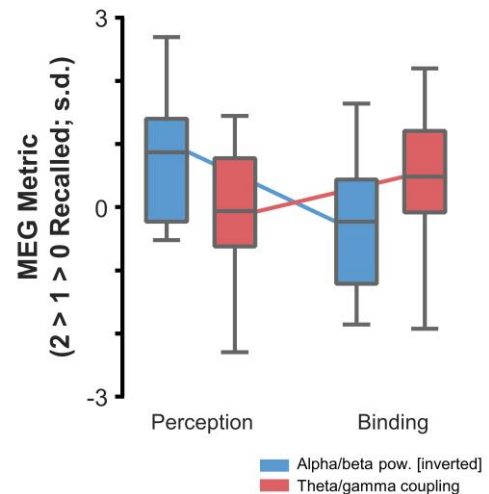


Figure 4. A temporal double dissociation between neocortical alpha/beta and hippocampal theta/gamma activity. Individual boxplots describe the effects of each task and each measure. The centre boxplot bar depicts the group mean, the box ends depict the 25th and 75th quartile and the tails depict the absolute minimum and maximum values within the sample. A significant interaction between the encoding stage and the MEG measure indicates that memory-related neocortical alpha/beta power decreases are most prominent during sequence perception, whereas memory-related increases in hippocampal theta/gamma coupling are most prominent during mnemonic binding.

387 window in which participants could mnemonically bind the sequence together. This double dissociation
388 suggests that alpha/beta power decreases and hippocampal theta/gamma phase-amplitude coupling arise
389 at two distinct stages in the memory formation process.

390 The representation of information relating to a to-be-encoded memory is thought to be supported by
391 neocortical alpha/beta power decreases (Hanslmayr et al., 2012). Information theory proposes that
392 unpredictable states, such as desynchronised neural networks, carry more information than predictable
393 states (Shannon & Weaver, 1949). In line with this hypothesis, we found that memory-related reductions in
394 alpha/beta power (an index for neural desynchrony) only arose when participants were required to process
395 information about a sequence, and not when the sequence was being bound together (i.e., when no further
396 information was presented for processing). The restriction of alpha/beta power decreases to time points
397 where information can be processed adds further support to the idea that alpha/beta power decreases
398 correlate with the representation of information relevant to episodic memories (Griffiths, Mayhew, et al.,
399 2019; Hanslmayr et al., 2012).

400 During mnemonic binding, hippocampal theta-gamma phase-amplitude coupling scaled with memory
401 performance. Mechanistically speaking, these increases may reflect a heightened degree of long-term
402 potentiation (LTP) within the hippocampus. By coupling gamma oscillations resonating at a frequency
403 optimal for spike-timing dependent plasticity (STDP; Bi & Poo, 1998; Nyhus & Curran, 2010) to the phase of
404 theta optimal for LTP (Hasselmo et al., 2002), the potential for building synaptic connections between
405 hippocampal neurons is increased greatly. Based on such ideas, one could speculate that the memory-
406 related theta-gamma coupling observed during the binding window reflects the transformation of the three
407 discrete sequence stimuli into a singular cohesive episodic memory. Similarly, the absence of memory-
408 related theta-gamma coupling during sequence perception may be attributable to the fact that the
409 sequence is still unfolding, and, as such, a cohesive representation of all three stimuli cannot yet be formed.
410 Notably, this is not to say that no theta-gamma coupling unfolds during sequence perception (indeed,
411 several frameworks and empirical studies propose the opposite; Bahramisharif, Jensen, Jacobs, & Lisman,
412 2018; Griffiths & Fuentemilla, 2019; Heusser, Poeppel, Ezzyat, & Davachi, 2016; Lisman & Jensen, 2013),
413 but rather, any theta-gamma coupling that does arise during that window is not predictive of later memory
414 performance in this particular task. Perhaps instead, such coupling is predictive of item-context binding (e.g.
415 Howard & Kahana, 2002), a measure not assessable here.

416 If these two phenomena are dissociable, does this mean that they act in complete independence of
417 one another during encoding? Here, we would argue “no”. Mnemonic binding cannot occur if the relevant
418 information has not been perceived, as there is no information to bind. Therefore, one could expect that
419 the underlying neural correlates of mnemonic binding are contingent on the prior neural processing of
420 relevant information. In line with such ideas, prior work has shown that the magnitude of hippocampal
421 gamma synchronisation can be predicted by preceding neocortical alpha/beta power decreases (Griffiths,
422 Parish, et al., 2019; see supplementary figure 4 for complementary findings within the data reported here).
423 As such, one could speculate that neocortical desynchrony and hippocampal synchrony correlate with
424 distinct cognitive processes (as evidenced above), but both neural phenomena (and the associated cognitive
425 processes) must arise and interact to create an episodic memory.

426 We did not observe any memory-related fluctuations in theta power during the binding window. This
427 is somewhat surprising; numerous previous studies have reported fluctuations in theta power correlating
428 with later memory performance (for reviews, Herweg et al., 2019; Nyhus & Curran, 2010). Given that
429 theories regarding theta and long-term potentiation (Bi & Poo, 1998; Hanslmayr et al., 2016; Nyhus &
430 Curran, 2010) emphasise the importance of phase for LTP, rather than power, one could speculate that
431 theta power has less to do with enhanced mnemonic binding, and as such, should not substantially correlate

432 with successful memory formation. Similarly, we did not observe fluctuations in gamma power during
433 mnemonic binding despite numerous studies demonstrating this previously (Burke et al., 2013; Griffiths,
434 Parish, et al., 2019; Long & Kahana, 2015; Osipova et al., 2006). However, this can be explained by the fact
435 that theta-gamma coupling was observed during this same window. If memory-related increases in gamma
436 power are restricted to certain phases of theta, and theta is not stimulus-locked across trials, then across-
437 trial averages of gamma power will sum to zero. As such, the absence of a ‘pure’ gamma effect here is not
438 surprising.

439 In sum, these results demonstrate that decreases in neocortical alpha/beta power and increases in
440 hippocampal theta/gamma phase-amplitude coupling are temporally dissociable in episodic memory
441 formation (Hanslmayr et al., 2016).

442 References

- 443 Aru, J., Priesemann, V., Wibral, M., Lana, L., Pipa, G., Singer, W., & Vicente, R. (2014). Untangling cross-frequency
444 coupling in neuroscience. *Current Opinion in Neurobiology*, 31(September 2014), 51–61.
445 <https://doi.org/10.1101/005926>
- 446 Bahramisharif, A., Jensen, O., Jacobs, J., & Lisman, J. (2018). Serial representation of items during working memory
447 maintenance at letter-selective cortical sites. *PLoS Biology*, 171660. <https://doi.org/10.1101/171660>
- 448 Bi, G., & Poo, M. (1998). Synaptic modifications in cultured hippocampal neurons: Dependence on spike timing,
449 synaptic strength, and postsynaptic cell type. *Journal of Neuroscience*, 18(24), 1–9.
450 <https://doi.org/10.1038/25665>
- 451 Burke, J. F., Zaghoul, K. a., Jacobs, J., Williams, R. B., Sperling, M. R., Sharan, a. D., & Kahana, M. J. (2013).
452 Synchronous and asynchronous theta and gamma activity during episodic memory formation. *Journal of*
453 *Neuroscience*, 33(1), 292–304. <https://doi.org/10.1523/JNEUROSCI.2057-12.2013>
- 454 Dalal, S., Jerbi, K., Bertrand, O., Adam, C., Ducorps, A., Schwartz, D., Martinerie, J., & Lachaux, J.-P. (2013).
455 Simultaneous MEG-intracranial EEG: New insights into the ability of MEG to capture oscillatory modulations in
456 the neocortex and the hippocampus. *Epilepsy and Behavior*, 28(2), 283–302.
457 <https://doi.org/10.1016/j.yebeh.2013.03.012>
- 458 Fellner, M.-C., Bäuml, K.-H. T., & Hanslmayr, S. (2013). Brain oscillatory subsequent memory effects differ in power
459 and long-range synchronization between semantic and survival processing. *NeuroImage*, 79, 361–370.
460 <https://doi.org/10.1016/j.neuroimage.2013.04.121>
- 461 Griffiths, B. J., & Fuentemilla, L. (2019). Event conjunction: How the hippocampus integrates episodic memories
462 across event boundaries. *Hippocampus*, 1–15. <https://doi.org/10.1002/hipo.23161>
- 463 Griffiths, B. J., Martín-Buro, M. C., Staresina, B. P., Hanslmayr, S., & Staudigl, T. (2021). Alpha/beta power decreases
464 during episodic memory formation predict the magnitude of alpha/beta power decreases during subsequent
465 retrieval. *Neuropsychologia*, 153(2021), 107755. <https://doi.org/10.1101/2020.07.08.193763>
- 466 Griffiths, B. J., Mayhew, S. D., Mullinger, K. J., Jorge, J., Charest, I., Wimber, M., & Hanslmayr, S. (2019). Alpha/beta
467 power decreases track the fidelity of stimulus-specific information. *ELife*, 8(e49562), 1–22.
468 <https://doi.org/10.32470/ccn.2019.1199-0>
- 469 Griffiths, B. J., Parish, G., Roux, F., Michelmann, S., Plas, M. Van Der, Kolibius, D., Chelvarajah, R., Rollings, D. T.,
470 Sawlani, V., Hamer, H., Gollwitzer, S., Kreiselmeyer, G., Staresina, B. P., Wimber, M., & Hanslmayr, S. (2019).
471 Directional coupling of slow and fast hippocampal gamma with neocortical alpha/beta oscillations in human
472 episodic memory. *Proceedings of the National Academy of Sciences*, 1–9.
473 <https://doi.org/10.1073/pnas.1914180116>
- 474 Haller, M., Donoghue, T., Peterson, E., Varma, P., Sebastian, P., Gao, R., Noto, T., Knight, R. T., Shestyuk, A., & Voytek,
475 B. (2018). Parameterizing neural power spectra. *BioRxiv*, 299859. <https://doi.org/10.1101/299859>
- 476 Hanslmayr, S., Matuschek, J., & Fellner, M.-C. (2014). Entrainment of prefrontal beta oscillations induces an
477 endogenous echo and impairs memory formation. *Current Biology*, 24(8), 904–909.
478 <https://doi.org/10.1016/j.cub.2014.03.007>

- 479 Hanslmayr, S., Staresina, B. P., & Bowman, H. (2016). Oscillations and episodic memory – Addressing the
480 synchronization/desynchronization conundrum. *Trends in Neurosciences*, *39*(1), 16–25.
481 <https://doi.org/10.1016/j.tins.2015.11.004>
- 482 Hanslmayr, S., & Staudigl, T. (2014). How brain oscillations form memories--a processing based perspective on
483 oscillatory subsequent memory effects. *NeuroImage*, *85 Pt 2*, 648–655.
484 <https://doi.org/10.1016/j.neuroimage.2013.05.121>
- 485 Hanslmayr, S., Staudigl, T., & Fellner, M.-C. (2012). Oscillatory power decreases and long-term memory: the
486 information via desynchronization hypothesis. *Frontiers in Human Neuroscience*, *6*(74), 1–12.
487 <https://doi.org/10.3389/fnhum.2012.00074>
- 488 Hasselmo, M. E., Bodelón, C., & Wyble, B. P. (2002). A proposed function for hippocampal theta rhythm: Separate
489 phases of encoding and retrieval enhance reversal of prior learning. *Neural Computation*, *14*(4), 793–817.
490 <https://doi.org/10.1162/089976602317318965>
- 491 Herweg, N. A., Solomon, E. A., & Kahana, M. J. (2019). Theta oscillations in human memory. *Trends in Cognitive
492 Sciences*, 1–20. <https://doi.org/10.1016/j.tics.2019.12.006>
- 493 Heusser, A. C., Poeppel, D., Ezzyat, Y., & Davachi, L. (2016). Episodic sequence memory is supported by a theta-
494 gamma phase code. *Nature Neuroscience*, *19*(August). <https://doi.org/10.1038/nn.4374>
- 495 Howard, M. W., & Kahana, M. J. (2002). A distributed representation of temporal context. *Journal of Mathematical
496 Psychology*, *46*(3), 269–299. <https://doi.org/10.1006/jmps.2001.1388>
- 497 Jutras, M. J., Fries, P., & Buffalo, E. A. (2009). Gamma-Band Synchronization in the Macaque Hippocampus and
498 Memory Formation. *Journal of Neuroscience*, *29*(40), 12521–12531. [https://doi.org/10.1523/JNEUROSCI.0640-
09.2009](https://doi.org/10.1523/JNEUROSCI.0640-
499 09.2009)
- 500 Karlsson, A. E., Wehrspau, C. C., & Sander, M. C. (2020). Item recognition and lure discrimination in younger and
501 older adults are supported by alpha/beta desynchronization. *Neuropsychologia*, *148*.
502 <https://doi.org/10.1101/2020.04.22.055764>
- 503 Kutner, M. H., Nachtsheim, C. J., & Neter, J. (2004). *Applied Linear Regression Models* (4th ed.). McGraw-Hill Irwin.
- 504 Lakens, D. (2013). Calculating and reporting effect sizes to facilitate cumulative science: A practical primer for t-tests
505 and ANOVAs. *Frontiers in Psychology*, *4*(NOV). <https://doi.org/10.3389/fpsyg.2013.00863>
- 506 Lisman, J. E., & Jensen, O. (2013). The theta-gamma neural code. *Neuron*, *77*(6), 1002–1016.
507 <https://doi.org/10.1016/j.neuron.2013.03.007>
- 508 Long, N. M., & Kahana, M. J. (2015). Successful memory formation is driven by contextual encoding in the core
509 memory network. *NeuroImage*, *119*, 332–337. <https://doi.org/10.1016/j.neuroimage.2015.06.073>
- 510 Manning, J. R., Jacobs, J., Fried, I., & Kahana, M. J. (2009). Broadband shifts in local field potential power spectra are
511 correlated with single-neuron spiking in humans. *Journal of Neuroscience*, *29*(43), 13613–13620.
512 <https://doi.org/10.1523/JNEUROSCI.2041-09.2009>
- 513 Maris, E., & Oostenveld, R. (2007). Nonparametric statistical testing of EEG- and MEG-data. *Journal of Neuroscience
514 Methods*, *164*(1), 177–190. <https://doi.org/10.1016/j.jneumeth.2007.03.024>
- 515 Martín-Buro, M. C., Wimber, M., Henson, R. N., & Staresina, B. P. (2020). Alpha rhythms reveal when and where item
516 and associative memories are retrieved. *Journal of Neuroscience*, *40*(12), 2510–2518.
517 <https://doi.org/10.1523/JNEUROSCI.1982-19.2020>
- 518 Nyhus, E., & Curran, T. (2010). Functional role of gamma and theta oscillations in episodic memory. *Neuroscience and
519 Biobehavioral Reviews*, *34*(7), 1023–1035. <https://doi.org/10.1016/j.neubiorev.2009.12.014>
- 520 Oostenveld, R., Fries, P., Maris, E., & Schoffelen, J.-M. (2011). FieldTrip: Open source software for advanced analysis
521 of MEG, EEG, and invasive electrophysiological data. *Computational Intelligence and Neuroscience*, *2011*, 1–9.
522 <https://doi.org/10.1155/2011/156869>
- 523 Osipova, D., Takashima, A., Oostenveld, R., Fernandez, G., Maris, E., & Jensen, O. (2006). Theta and gamma
524 oscillations predict encoding and retrieval of declarative memory. *Journal of Neuroscience*, *26*(28), 7523–7531.
525 <https://doi.org/10.1523/JNEUROSCI.1948-06.2006>
- 526 Ruzich, E., Crespo-García, M., Dalal, S. S., & Schneiderman, J. F. (2019). Characterizing hippocampal dynamics with
527 MEG: A systematic review and evidence-based guidelines. *Human Brain Mapping*, *40*(4), 1353–1375.

- 528 <https://doi.org/10.1002/hbm.24445>
- 529 Sederberg, P. B., Schulze-Bonhage, A., Madsen, J. R., Bromfield, E. B., McCarthy, D. C., Brandt, A., Tully, M. S., &
530 Kahana, M. J. (2007). Hippocampal and neocortical gamma oscillations predict memory formation in humans.
531 *Cerebral Cortex*, 17(5), 1190–1196. <https://doi.org/10.1093/cercor/bhl030>
- 532 Shannon, C. E., & Weaver, W. (1949). *A mathematical theory of communication*. University of Illinois Press.
- 533 Staudigl, T., & Hanslmayr, S. (2013). Theta oscillations at encoding mediate the context-dependent nature of human
534 episodic memory. *Current Biology*, 23(12), 1101–1106.
- 535 Tort, A. B. L., Komorowski, R., Eichenbaum, H., & Kopell, N. (2010). Measuring phase-amplitude coupling between
536 neuronal oscillations of different frequencies. *Journal of Neurophysiology*, 104(2), 1195–1210.
537 <https://doi.org/10.1152/jn.00106.2010>
- 538 Tort, A. B. L., Komorowski, R. W., Manns, J. R., Kopell, N. J., & Eichenbaum, H. (2009). Theta-gamma coupling
539 increases during the learning of item-context associations. *Proceedings of the National Academy of Sciences*,
540 106(49), 20942–20947. <https://doi.org/10.1073/pnas.0911331106>
- 541 Tulving, E. (2002). Episodic memory: from mind to brain. *Annual Review of Psychology*, 53, 1–25.
542 <https://doi.org/10.1146/annurev.psych.53.100901.135114>
- 543 van Veen, B., van Drongelen, W., Yuchtman, M., & Suzuki, A. (1997). Localization of brain electrical activity via linearly
544 constrained minimum variance spatial filtering. *IEEE Transactions on Biomedical Engineering*, 44(9), 867–880.
545 <https://doi.org/10.1109/10.623056>
- 546 Zhang, H., & Jacobs, J. (2015). Traveling theta waves in the human hippocampus. *Journal of Neuroscience*, 35(36),
547 12477–12487. <https://doi.org/10.1523/JNEUROSCI.5102-14.2015>
- 548